UC Berkeley
UC Berkeley Previously Published Works

Title
A Descriptor-Based Approach to Predict the Catalytic Activity of Zinc CO2 Hydration Catalysts

Permalink
https://escholarship.org/uc/item/4c993718

Journal
ACS Catalysis

ISSN
2155-5435

Authors
Quaid, Thomas
Citek, Cooper
Hartwig, John F
et al.

Publication Date
2026-10-23

DOI
10.1021/acscatal.6c03861

Supplemental Material
https://escholarship.org/uc/item/4c993718#supplemental

Copyright Information
This work is made available under the terms of a Creative Commons Attribution-NonCommercial-NoDerivatives License, available at https://creativecommons.org/licenses/by-nc-nd/4.0/

Peer reviewed

eScholarship.org Powered by the California Digital Library
University of California

ACS Catalysis

pubs.acs.org/acscatalysis Research Article

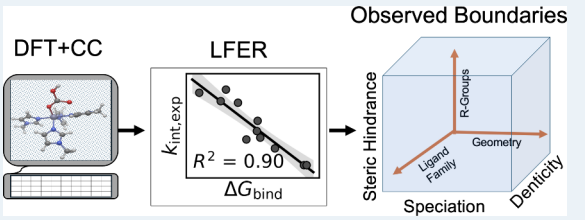
A Descriptor-Based Approach to Predict the Catalytic Activity of Zinc CO_2 Hydration Catalysts

Thomas Quaid, Cooper Citek, John F. Hartwig,* and Douglas S. Clark*

Cite This: *ACS Catal.* 2026, 16, 21140−21150 Read Online

ACCESS | Metrics & More | Article Recommendations | Supporting Information

ABSTRACT: Carbonic anhydrase (CA) catalyzes CO_2 hydration with turnover frequencies approaching 10^6 s^{-1}, but native enzymes lack stability under conditions typical of industrial carbon capture. Small-molecule zinc mimics can be more stable under harsh conditions, but product inhibition by bicarbonate limits efficiency. A general framework for predicting turnover across ligand scaffolds has remained elusive. We report the analysis, by experiment and computation, of speciation and catalytic activity of zinc complexes as CA mimics. A literature data set of twelve Zn-ligand complexes was constructed, and the binding free energy (ΔG_{bind}) of bicarbonate to zinc was calculated by DFT with DLPNO-CCSD(T) refinement. ΔG_{bind} strongly correlates with the intrinsic rate constants of these Zn-ligand complexes for CO_2 hydration with $R^2 = 0.90$ at pH 9, 25 °C, and saturated CO_2 (1 atm). By comparison, combining the commonly used descriptors $\Sigma E^{(2)}$, q_{Zn}, and $\%V_{buried}$ resulted in $R^2 = 0.74$. Examining additional Zn catalysts (for example, the coordination species $[ZnL_4(OH)]^+$, where L is 1-methylimidazole) revealed that chemical speciation must be accounted for to describe the observed dependence of catalytic activity on ligand stoichiometry. Furthermore, accurate ranking of catalytic activity for several of the modified cyclens considered requires accounting for steric congestion ($\%V_{buried}$), as ΔG_{bind} alone does not capture active-site occlusion. These results define a transferable framework that integrates ΔG_{bind}, speciation, and steric properties to enable the design of Zn-based CO_2 hydration catalysts.



KEYWORDS: *carbonic anhydrase mimic, zinc-mediated CO_2 hydration, speciation-corrected modeling, ΔG_{bind} descriptor, macrocyclic ligands, DFT catalysis modeling*

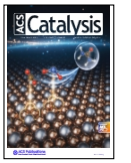
1. INTRODUCTION

Metalloenzymes provide inspiration for the development of synthetic molecular inorganic catalysts that react with high activity and selectivity under mild conditions.[1−3] A flagship example of metalloenzymatic efficiency is carbonic anhydrase (CA), which catalyzes the hydration of carbon dioxide to bicarbonate with diffusion-limited turnover frequencies approaching 10^6 s^{-1}.[4−6] These turnover frequencies remain unmatched by synthetic analogs. The active site of CA is a tetrahedral Zn^{2+} center coordinated by three histidine residues and a water molecule, which, upon deprotonation, forms a highly reactive Zn−OH species.[6,7] Carbonic anhydrases with substantial thermal and alkaline stability have been obtained by protein engineering and metagenomic mining of samples from high-temperature environments, and these variants have been evaluated for carbon capture.[8,9] Remaining limitations include durability over required operating lifetimes and economical production and immobilization of the enzymes at scale.[10] Consequently, robust small-molecule mimics have been sought as complementary catalyst platforms.[10,11]

The pursuit of abiotic CA mimics spans more than half a century, from early efforts involving cobalt complexes of tetraazacyclododecane or tris-imidazole phosphine scaffolds[12,13] to more elaborate zinc complexes engineered to engender secondary-sphere hydrogen-bonding interactions.[14] However, product inhibition, due to the accumulation of bicarbonate, remains a prevailing challenge.[15] Rains et al.[15] introduced ZnL1S (structure shown in Figure 1) as a high-performance mimic, reporting reaction rate constants that change sharply with varying concentrations of CO_2, bicarbonate, and with pH.

Prior work indicates that rates of reactions catalyzed by Zn-based small-molecule CA mimics can be limited by addition of CO_2 or release of bicarbonate from the bicarbonate complex. Kim and Kulik computed the complete pathway for $Zn(imi)_3$ and identified CO_2 addition and bound bicarbonate as the turnover-determining transition state and intermediate, respectively.[16] In addition, Koziol et al.[17] provided theoretical and experimental evidence that release of bicarbonate may be the

Received: May 19, 2026
Revised: October 8, 2026
Accepted: October 9, 2026
Published: October 23, 2026



ACS Publications © 2026 American Chemical Society

https://doi.org/10.1021/acscatal.6c03861
ACS Catal. 2026, 16, 21140−21150

Downloaded from pubs.acs.org/acscatal/article-pdf/16/21/21140/6896732/cs-2026-038616.pdf by UNIV OF CALIFORNIA BERKELEY user on 13 November 2026

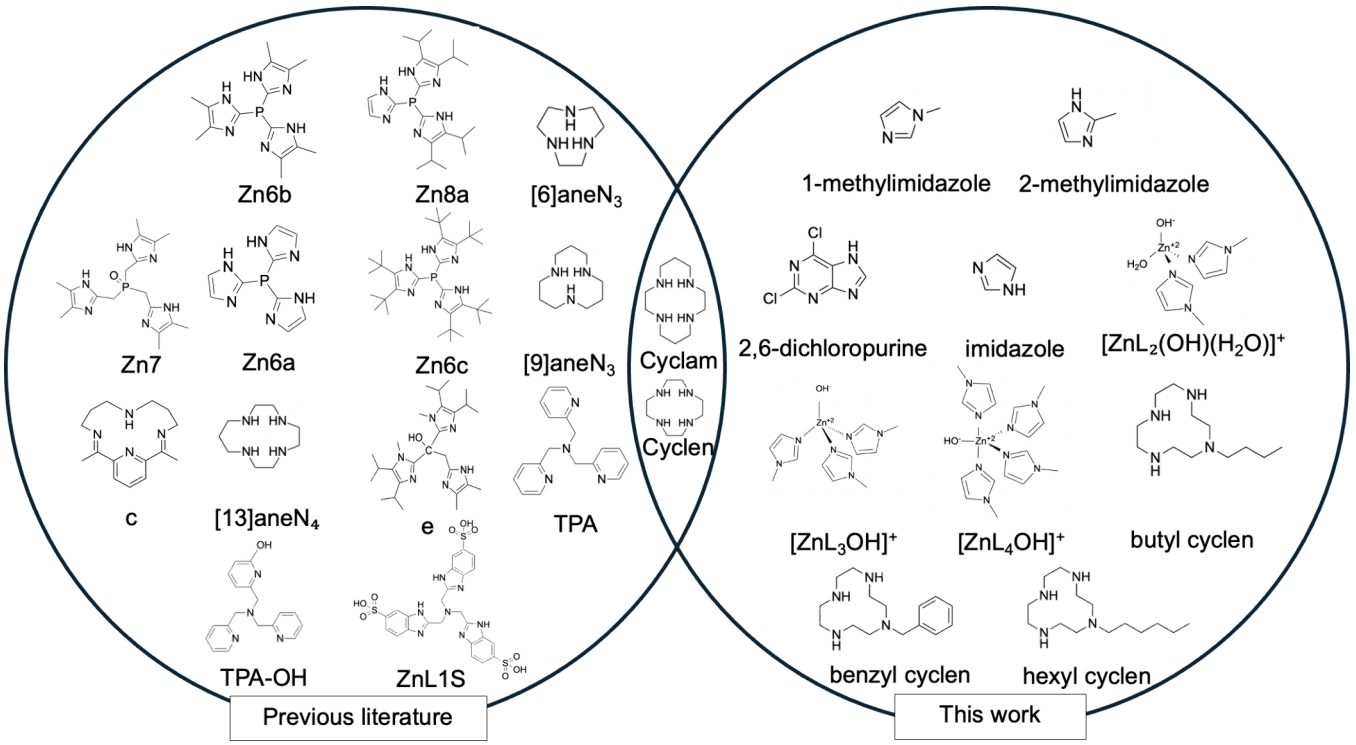


Figure 1. Previously experimentally explored ligands versus those in this work, outlining the molecules for which experimental rate constants were obtained from the literature and those measured in this work. Cyclen and cyclam were used as literature comparisons for our analysis to benchmark our experimental methods.

rate-limiting step of CO_2 hydration catalyzed by zinc complexes of aza-macrocyclic ligands. Rains et al.[15] used a variety of methods to assign the bicarbonate-bound intermediate step as rate-limiting in the dehydration of bicarbonate catalyzed by ZnL1S. Together, these studies indicate that the free energy for dissociation of bicarbonate from the complex correlates with the rate constant for CO_2 hydration by multiple Zn mimics, but they do not establish a single rate-determining step across ligand classes.

Ab initio predictions of thermodynamic and kinetic properties of molecular systems have improved substantially in accuracy and computational efficiency over the past decade. As a result, significant progress has been made in the rational design of synthetic and biomimetic catalysts across diverse applications.[18,19] Descriptor-based computational modeling has provided a framework to interrogate and predict the performance of CA mimics by reducing computational costs of evaluating complex systems.[16,20] Density-functional theory (DFT) and local-correlation methods have enabled the quantification of thermodynamic and electronic parameters, such as the Zn-bicarbonate binding energy (ΔG_{bind}), metal-centered charge (q_{Zn}),[21] donor-acceptor interaction energies ($\Sigma E^{(2)}$),[22] and the steric accessibility of the active site ($\%V_{buried}$).[23,24] Through the combined use of DFT and DLPNO-CCSD(T) single-point refinement, accurate modeling can be extended to systems that are otherwise intractable to calculations with full coupled-cluster theory, improving predictive accuracy, as demonstrated here.

We introduce a protocol based on molecular descriptors, corrected for speciation, for modeling and evaluating the catalytic efficiencies of a structurally diverse array of zinc coordination motifs. Conventional implementations of models to interrogate CA mimics have often failed to account for speciation, particularly for systems bearing monodentate ligands. Our findings also show that excess ligand:Zn stoichiometries can be modeled to improve agreement with observed rate constants, providing a useful design variable beyond ligand identity alone.

By integrating quantum mechanical modeling, speciation corrections, and experimental rate constants, this study presents a descriptor-based framework for predicting catalytic performance in zinc CO_2 hydration catalysts. Because the workflow is based on ground-state energy evaluations, it avoids explicit transition-state optimizations, which are often computationally prohibitive for larger data sets. While full microkinetic models can capture coupled reaction networks and dynamic system behavior, they require extensive parameterization and system-specific assumptions. Here, we instead employ a descriptor-based framework augmented with equilibrium speciation, capturing the dominant thermodynamic and compositional effects governing observed activity, while retaining interpretability across Zn-based CA mimics.

2. COMPUTATIONAL DETAILS

All quantum chemical and thermodynamic calculations were performed using an internally developed, descriptor-based high-throughput platform, termed QUARKS (QUAntum woRKflow Suite), which automates conformer searches, geometry optimizations, energy refinements, and descriptor extraction for large sets of ligands across multiple ligand classes. The suite of programs includes several open-access programs, such as ORCA[25,26] and Molassembler[27] with newly generated graphical user interfaces (GUIs). Ligands were first constructed

Downloaded from pubs.acs.org/acscatsc/article-pdf/16/21/21140/6896732/cs-2026-038616.pdf by UNIV OF CALIFORNIA BERKELEY user on 13 November 2026

https://doi.org/10.1021/acscatal.6c03861
ACS Catal. 2026, 16, 21140−21150

in Avogadro2 and then subjected to a conformational search using GFN2-xTB,[28] ALPB water solvation, and CREST.[29] DFT geometry optimizations were performed at the B3LYP-D4/def2-SVP level using CPCM solvation (water), followed by frequency calculations and single-point energy evaluations at B3LYP-D4/def2-TZVPP. A visual protocol is available in Figure S1.

2.1. Descriptor Development

To develop an accurate procedure for modeling zinc complexes, we curated a benchmark activity data set comprising zinc complexes of five ligands (**M1**−**M5**) reported by Koziol et al.,[17] selected for internal consistency and for the availability of experimental rate constants. This method-benchmarking set allowed us to isolate method performance without inter-laboratory variability. Ten computational methods with DFT were tested, spanning functionals, basis sets, dispersion corrections, and solvation treatments described in Table S2. For each procedure, the Zn-bicarbonate binding energy (ΔG_{bind}), relative to the vacant Zn complex and free bicarbonate anion (eq S1), was computed and correlated with intrinsic rate constants ($k_{int,exp}$) obtained by accounting for the fraction of catalytically active Zn-OH at the experimental pH (see Supporting Information) for **M1**−**M5**.

Published rate constants for identical Zn-cyclen and Zn-cyclam catalysts span approximately one order of magnitude across laboratories (Table S1), even among studies that used the same stopped-flow spectroscopic method and originated from the same lab. All rate constants in this work, therefore, were normalized to a consistent set of pre-reaction conditions (before 1:1 stopped-flow mixing: [Zn] ≤ 1 mM in buffered pH 9 solution; saturated CO_2 in water at 1 atm; 25 °C) prior to regression.

Among the protocols tested, B3LYP/def2-TZVPP with D4 dispersion and CPCM(water) solvation was selected as a practical compromise from the limited five-complex benchmark. It gave R^2 = 0.86, MAE = 532 M^{-1} s^{-1}, RMSE = 617 M^{-1} s^{-1}, Q^2_{LOO} = 0.58, and MAE_{CV} = 940 M^{-1} s^{-1}. DLPNO-CCSD(T)/def2-TZVPP single-point corrections were then applied to the DFT-optimized geometries and frequencies, giving R^2 = 0.91 for the benchmark data set (Figure 2).

The final procedure and speciation model were validated using an independent data set of twelve ligands drawn from multiple literature sources (Table 1), excluding the five datapoints used in the benchmarking study above (Figure 2). This external set encompasses a range of ligand families (macrocyclic and scorpionate), denticities (tetra- and tridentate), and intrinsic rate constants ranging from zero to 868 M^{-1} s^{-1}. The agreement between the predicted ΔG_{bind} values and experimentally derived $k_{int,exp}$ values across both the benchmark and model sets forms the foundation for the modeling, screening, and mechanistic analyses presented in the following sections.

ΔG_{bind} is the computed free energy for dissociation of bicarbonate from each Zn−ligand complex (eq S1). A larger value denotes stronger binding. It is a ground-state quantity that does not describe transition states or speciation in solution and is used here to rank the complexes within the sampled set.

2.2. Normalization for the Fraction of Catalytically Active Zn−OH

Each literature k_{obs} value in this study was converted to the intrinsic rate constant ($k_{int,exp}$) by accounting for the fraction of Zn present as the catalytically active Zn-OH species at the experimental pH through the procedures outlined in the Supporting Information section titled "Normalization of Rate Constants Using the Fraction of Catalytically Active Zn−OH." Protonation states and speciation were addressed by predicting ligand pK_a values from the optimized Zn−OH bond lengths by a previously reported method using a linear model trained on an expanded combination of experimental and calculated values from Koziol et al., available in Table S3. The resulting fit, $pK_a = 43.34 \cdot (d_{Zn-O}) - 74.42$, reproduced benchmark p$K_a$ values with R^2 = 0.82 (Figure S4). The fraction of active catalyst (f_{OH}) was then determined using the Henderson−Hasselbalch relation (eq S2 in the Supporting Information).

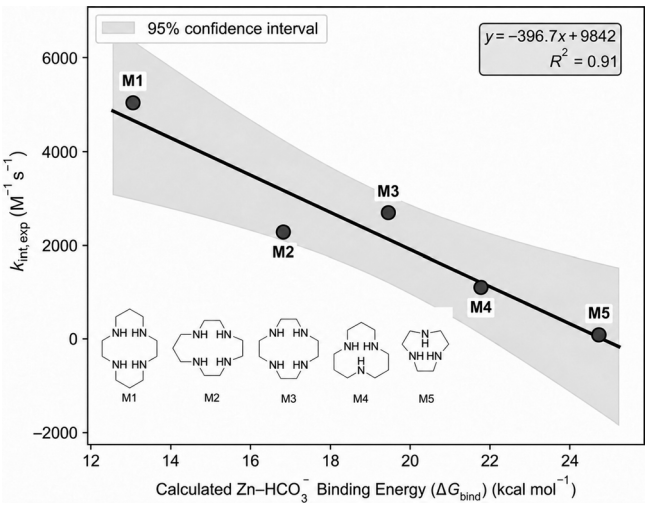


Figure 2. Correlation between computed Zn−bicarbonate binding free energies (ΔG_{bind}) and experimentally determined intrinsic rate constants ($k_{int,exp}$) for the five macrocyclic CA mimics **M1**−**M5** reported by Koziol et al.[17] The $k_{int,exp}$ values were reported for uniform assay conditions (pH 9, 25 °C, saturated CO_2, 1 atm). The solid trendline shows the least-squares fit (R^2 = 0.91), illustrating the inverse relationship between turnover and Zn-bicarbonate affinity.

2.3. Steric Evaluation

Steric parameters were computed to test whether ground-state congestion, in addition to ΔG_{bind}, contributes to the prediction of $k_{int,pred}$, as discussed in Section 3. Steric congestion was quantified by the SambVca protocol originally reported by Poater et al.[24] A 4.0 Å sphere centered on zinc was selected after sensitivity analysis (2.5−5.0 Å) identified this radius as most accurately reproducing the experimental ranking of activities. Conformer ensembles generated with GFN2-xTB/ALPB(water)/GOAT[33] from the ORCA framework were Boltzmann-weighted at 298 K; the reported $\%V_{buried}$ values are ensemble averages.

3. RESULTS AND DISCUSSION

3.1. ΔG_{bind} as a Transferable Predictor of Intrinsic Catalytic Activity

Using the computational protocol described above, the data from Koziol et al. with ligands **M1**−**M5** provided a rigorously controlled data set (identical buffer, CO_2 loading, temperature,

Downloaded from pubs.acs.org/acscatal/article-pdf/16/21/21140/6896732/cs-2026-038616.pdf by UNIV OF CALIFORNIA BERKELEY user on 13 November 2026

https://doi.org/10.1021/acscatal.6c03861
ACS Catal. 2026, 16, 21140−21150

Table 1. Reported Measured and pH-Corrected Rate Constants and Zn−HCO_3 Binding Free Energies for Specified Zn-Ligand Complexes

ligand complex (source identifiers)	$k_{int,exp}$ (M^{-1} s^{-1})	k_{obs} (M^{-1} s^{-1})	binding energy Zn-HCO_3 (DFT) (kcal mol^{-1})	binding energy Zn−HCO_3 (DFT + CC) (kcal mol^{-1})	source
cyclam (**M1**)	868	126	12.8	13.1	30
Zn6c	832	626	9.1	10.0	31
TPA-OH	735	735	12.7	12.5	14
TPA	718	648	14.7	14.5	14
cyclen (**M3**)	508	471	17.9	16.8	30
Zn7	392	156	16.6	16.7	12
e	316	240	17.2	17.1	32
c	296	225	14.2	15.5	31
ZnL1S	191	86	20.0	18.8	15
Zn6a	0	0	25.5	22.5	31
Zn6b	0	0	24.1	22.2	31
Zn8a	0	0	24.3	22.5	31

and zinc concentration) to calibrate our benchmarking study. Across ten combinations of functional, basis set, solvation method, and dispersion corrections, ΔG_{bind} computed with B3LYP-D4/def2-TZVPP + DLPNO-CCSD(T) (DFT + CC) aligned most closely with the intrinsic rate constants, with $R^2 = 0.91$. The computed ΔG_{bind} values spanned 12 kcal mol^{-1} across the five ligands. This correlation supports the use of the Zn-bicarbonate binding free energy as a predictor of the rate constant, but it does not identify one universal turnover-limiting elementary step.

The transferability of the model to structurally diverse ligands proved equally strong: when the model trained on the five macrocyclic complexes was applied to a set of twelve ligands (Figure 3; Table 1), the correlation between computed Zn-bicarbonate binding free energy and measured rate constant remained high ($R^2 = 0.90$). This set includes varied ligand scaffolds, such as macrocyclic tetraamines and tripodal phosphorus- and nitrogen-donor scorpionates representing tri- and tetradentate ligands. Within the sampled set, these results support ΔG_{bind} as an empirical predictor of the rate constants of Zn-catalyzed CO_2 hydration. Correlations between $k_{int,exp}$ and bicarbonate binding energies computed by DFT alone (B3LYP-D4/def2-TZVPP, CPCM(water)) were weaker for this 12-ligand set ($R^2 = 0.79$) than the correlation obtained with DFT + CC (DLPNO-CCSD(T) single-point energies; $R^2 = 0.90$, $\Delta R^2 = +14\%$, $\Delta RMSE = -29\%$, and $\Delta MAE = -33\%$). Metric comparisons are available in Table S7 of the Supporting Information. Subsequent predictions of intrinsic rate constants from ΔG_{bind} use the linear regression in Figure 3 within the range of ΔG_{bind} sampled.

The data set reported by Koziol et al.[17] exhibits internally consistent trends across ligands but is systematically offset in absolute magnitude relative to other literature sources and our own measurements.[31] As a result, inclusion of these data in a pooled regression distorts the global ΔG_{bind}–$k_{int,exp}$ relationship despite preserving relative ordering. Accordingly, the data of Koziol et al. are used for internal benchmarking (Figure 2), but they are excluded from cross-study regression analyses (Figure 3).

The approximate linearity of the correlations in Figures 2 and 3 reflects an empirical observation that applies over the range of parameters included in our analysis and is not derived from a kinetic model. However, it is consistent with the linear free energy relationship reported by Kim and Kulik for their

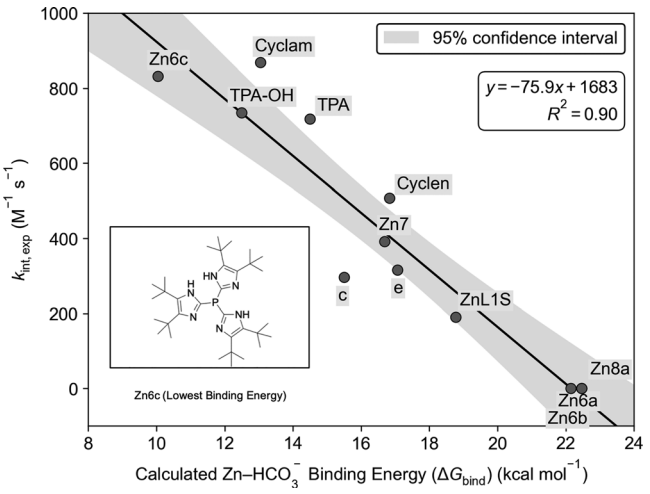


Figure 3. Correlation between predicted Zn-bicarbonate binding free energy (ΔG_{bind}) and experimentally derived intrinsic catalytic rate constants ($k_{int,exp}$) for CO_2 hydration by a set of twelve literature-reported Zn-ligand complexes. All data were recalibrated to standardized conditions of pH 9 using the Henderson-Hasselbalch normalization protocol. Error bars for the y-axis are omitted due to inconsistent reporting and error handling from the original sources, which may foster misleading comparisons. (Inset) ligand with the highest reported $k_{int,exp}$ (868 $M^{-1}s^{-1}$) to date for pH-corrected and consistent [CO_2]. Data, ligands, sources, and comparisons of DFT vs DFT + CC derived binding free energies are available in Table 1. The data of Koziol et al.[17] are not included in this regression, due to a systematic offset between the reported rate magnitudes and other literature data sets (see Section 3 and the Supporting Information for details).

computed cycles for hydration of CO_2 by $Zn(imi)_3$ and three of its derivatives.[16] Furthermore, over the 8.8 kcal mol^{-1} range of ΔG_{bind} sampled here, the rate constants vary only 4.5-fold, so a linear dependence cannot be distinguished from an exponential dependence. The predictive ability of ΔG_{bind} requires that reaction-induced changes to coordination and speciation do not change the ordering of the complexes by ΔG_{bind}. The correlation with $k_{int,exp}$ indicates that this ordering is retained within the sampled set.

For the nine Zn complexes with measurable rate constants included in Figure 3, the R^2 value from a linear fit of $k_{int,exp}$ to ΔG_{bind} is 0.77, whereas the R^2 for all twelve complexes is 0.90.

https://doi.org/10.1021/acscatal.6c03861
ACS Catal. 2026, 16, 21140−21150

Downloaded from pubs.acs.org/acscatal/article-pdf/16/21/21140/6896732/cs-2026-038616.pdf by UNIV OF CALIFORNIA BERKELEY user on 13 November 2026

As one basis of comparison, the R^2 for these same nine complexes fitted to the exponential function $k = a{\cdot}\exp(b{\cdot}\Delta G_{bind})$ is 0.69 (0.79 for all twelve). Furthermore, for the separate benchmark set of Koziol et al.[17] comprising five complexes, the R^2 value for the linear correlation between the experimental $k_{int,exp}$ values and ΔG_{bind} values calculated using the present protocol is 0.91 (Figure 2). However, this empirical relationship is not assumed to transfer beyond the sampled set.

3.2. Quantitative Limits of First-Coordination-Sphere Descriptors $\Sigma E^{(2)}$, q_{Zn}, and $\%V_{buried}$

To probe descriptor-based modeling beyond the general correlation between $k_{int,exp}$ and ΔG_{bind} (Figure 3, $R^2 = 0.90$), we evaluated three frequently used, chemically distinct first-coordination-sphere descriptors ($\Sigma E^{(2)}$, q_{Zn}, and $\%V_{buried}$) for the rigid multidentate ligands in Figure 3: (i) the Natural Bond Orbital (NBO) donor−acceptor second-order energy $\Sigma E^{(2)}$; (ii) the Zn NBO charge in the ligand-Zn complex q_{Zn}; and (iii) the percent buried volume of the Zn active site, $\%V_{buried}$. For (i) and (ii), see work from Glendening et al.[22] for derivations. The least-squares regression obtained by extracting these parameters from the structures in the model set and comparing with experimental rate constants is given by eq 1:

$$\ln k_{int,pred} = -10.3 + 0.15{\cdot}\Sigma E^{(2)} - 45.0{\cdot}q_{Zn} + 1.07{\cdot}\%V_{buried} \quad (1)$$

This regression provides a quantitative mapping between variations in the first-coordination-sphere descriptors ($\Sigma E^{(2)}$, q_{Zn}, and $\%V_{buried}$) and the catalytic rate constants within the model set. The correlation between the intrinsic (Zn−OH normalized), experimental value of ln $k_{int,exp}$ and the predicted value of ln $k_{int,pred}$ using this equation was $R^2 = 0.74$, with a leave-one-out cross-validated $R^2_{CV} = 0.43$. The three complexes with no measurable activity entered the regression as $k = 10^{-6}$ M^{-1} s^{-1}. A negative coefficient was obtained for q_{Zn} (−45.0), and this negative value indicates that accumulation of positive charge on Zn upon dissociation of bicarbonate inhibits turnover, whereas positive coefficients for $\Sigma E^{(2)}$ (+0.15) and $\%V_{buried}$ (+1.07) indicate that stronger ligand donor interactions and increased steric bulk modestly enhance rate constants. To interpret the relative influence of each descriptor, we refit the regression using z-normalized inputs. The standardized coefficient for $\%V_{buried}$ (+0.87) is the largest of the three, followed by those for q_{Zn} (−0.20) and $\Sigma E^{(2)}$ (+0.14). The contributions of $\Sigma E^{(2)}$ and q_{Zn} are consistent with stabilization of positive charge on Zn, facilitating bicarbonate dissociation. The contribution of $\%V_{buried}$ indicates that steric crowding around the zinc center facilitates displacement of the product. These inferences align with reported trends about the steric and electronic effects of ligands on nickel-based CO_2 fixation and Zn-based ring-opening polymerization of lactides.[34,35]

Within the sampled descriptor ranges, this regression bounds the rate constants predicted for Zn complexes of multidentate ligands. The values of the descriptors for the set of complexes spanned the following ranges: $\Sigma E^{(2)}$ = 164−198 kcal mol^{-1}, q_{Zn} = 1.66−1.77 e, and $\%V_{buried}$ = 39.9−65.2% (Table S5). Extrapolation to the favorable extremes of the descriptors ($\Sigma E^{(2)}$ = 198 kcal mol^{-1}, q_{Zn} = 1.66 e, $\%V_{buried}$ = 65.2%), leads to a value of ln $k \approx 13.4$ ($k \approx 6.7 \times 10^5$ M^{-1} s^{-1}). This value represents an estimated upper bound within the available descriptor values ($\Sigma E^{(2)}$, q_{Zn}, and $\%V_{buried}$) for the first coordination sphere of these ligands and exceeds the highest measured rate constant, 868 M^{-1} s^{-1} for the cyclam complex.

To assess whether these first-coordination-sphere descriptors add out-of-sample predictive information beyond ΔG_{bind}, ZnL1S was excluded because its first-coordination-sphere descriptors lie outside the range spanned by the other eleven complexes. A leave-one-complex-out LASSO analysis identified ΔG_{bind} as the only descriptor retained in all 11 folds of the four-descriptor model; full validation and sensitivity results are reported in the Supporting Information (Table S8).

Across the eleven complexes of Table 1 other than ZnL1S, $\%V_{buried}$ is associated with 55% of the variance in ΔG_{bind} ($p = 0.009$), but $\Sigma E^{(2)}$ and q_{Zn} together are associated with just 14%. These regressions reveal covariance within this data set and do not establish causal mechanisms. Adding $\%V_{buried}$ to the regression of $k_{int,exp}$ on ΔG_{bind} does not improve the prediction ($\Delta R^2 = 0.000$).

3.3. Evaluation of Complexes with Monodentate Ligands

We tested whether the ΔG_{bind} descriptor also correlates with the values of $k_{int,exp}$ for reactions catalyzed by complexes containing more labile monodentate ligands. A virtual screen of 30 monodentate *N*-heterocyclic ligand structures from the ChEMBL database was performed. The computed ΔG_{bind} values were converted to predicted rate constants ($k_{int,pred}$) from the linear correlation between ΔG_{bind} and $k_{int,exp}$ (Figure 3) derived from the 12-ligand model set (vide supra). The resulting distribution (ranked by the predicted rate constant) is shown in Figure 4, together with 1-methylimidazole (L16), which was added as a literature comparison. Compound identifiers are provided in Table S6.

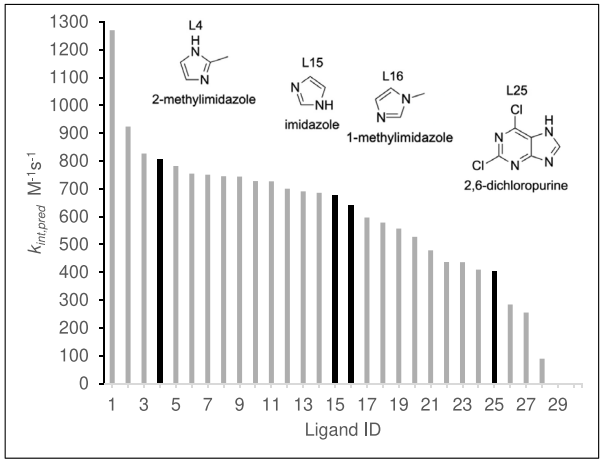


Figure 4. Predicted rate constants ($k_{int,pred}$) for 30 monodentate *N*-heterocyclic ligands (30 identified from the ChEMBL database and 1-methylimidazole). The structure of each of the zinc bicarbonate complexes was modeled using the validated B3LYP-D4/def2-TZVPP + DLPNO-CCSD(T) procedure, and the resulting ΔG_{bind} values were converted to predicted rate constants using the linear correlation established in Figure 3. Candidates were ranked in descending order of activity. Four ligands (compounds 4, 15, 16, and 25 highlighted in black and displayed in reported order as images) were selected for experimental validation. Corresponding ChEMBL identifiers and predicted rate constants are listed in Table S6.

Downloaded from pubs.acs.org/acscatal/article-pdf/16/21/21140/6896732/cs-2026-038616.pdf by UNIV OF CALIFORNIA BERKELEY user on 13 November 2026

https://doi.org/10.1021/acscatal.6c03861
ACS Catal. 2026, 16, 21140−21150

To evaluate the ability of this model to predict the reactivity of complexes containing monodentate ligands, we measured the experimental rate constants for reactions catalyzed by complexes of four imidazolic ligands, 2-methylimidazole (**L4**), imidazole (**L15**), 1-methylimidazole (**L16**), and 2,6-dichloropurine (**L25**). These ligands represent a range of predicted $k_{int,pred}$ across the modeled ligands. The rate constants observed for reactions with 4:1 ligand:Zn ratios (vide infra) under standard conditions, converted to pH-independent intrinsic rate constants, matched the predicted rank order by the model (Table 2), affirming the correlation of the intrinsic rate constants with the bicarbonate binding free energy for complexes of these monodentate ligands. As is commonly observed in descriptor-based analyses of catalytic activity, deviations from idealized single-descriptor correlations are expected when additional thermodynamic or compositional factors (such as speciation equilibria) are present.[36]

However, in all four cases, the intrinsic (Zn−OH normalized) experimental values $k_{int,exp}$ were approximately 15% of the predicted values. The 4:1 ligand:Zn ratio was chosen to bias the system toward zinc complexes with a higher number of *N*-heterocyclic ligands (3:1, 4:1 ligand:Zn) while minimizing contributions from complexes with a lower number of such ligands (1:1, 2:1 ligand:Zn). Under these conditions, multiple coordination numbers are expected to coexist, including ZnL_2, ZnL_3, and ZnL_4. The tris-ligated species was used as a representative catalytically active complex for modeling purposes, rather than a uniquely dominant solution species.

This simplification was initially motivated by analogy to carbonic anhydrase, where a tris-coordinate environment supports the catalytically relevant $[ZnL_3(OH)]^+$ motif, and all systems were modeled accordingly. The observed discrepancy between predicted and experimental rate constants therefore raises a mechanistic question: does the deviation reflect a limitation of the ΔG_{bind}-based model, or does it arise from solution speciation deviating from the assumed $[ZnL_3(OH)]^+$ stoichiometry in these labile Zn−ligand systems? This question is addressed quantitatively in the speciation analysis below.

3.4. Speciation Controls Observed Rates in Monodentate Systems

The systematic ∼7-fold discrepancy between predicted and observed rate constants for monodentate imidazole complexes at 4:1 ligand:Zn (Table 2) raised an important mechanistic question: does solution speciation deviate substantially from the assumed $[ZnL_3(OH)]^+$ stoichiometry, given the lability of monodentate Zn-ligand systems? We probed the differences between predicted and observed rate constants (Table 2) by further measuring the values of $k_{int,exp}$ of 1-methylimidazole:-zinc mixtures at molar ratios ranging from 3:1 to 250:1 at pH 9, saturated CO_2, 1 atm, and stock zinc concentrations of 1.0, 0.50, and 0.25 mM (see Experimental Procedures in the Supporting Information for further details). Figure 5 reveals a skewed bell-shaped profile of the experimentally observed rate constants for 1-methylimidazole (1-MIm) solution (k_{obs}): the activity increases sharply with ligand equivalents, reaching a maximum of ∼850 M^{-1} s^{-1} at a 15:1 ligand-to-metal ratio, then declines gradually. The model (solid line) captures the overall bell-shaped dependence of activity on the ligand:Zn ratio.

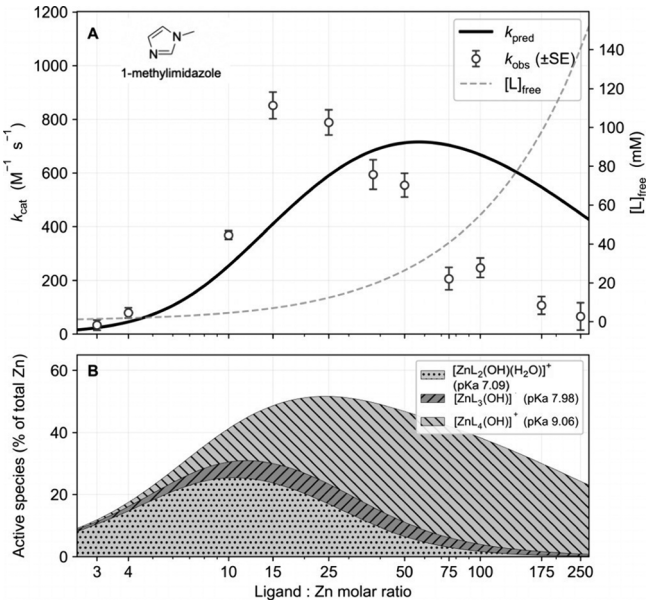


Figure 5. (A) Experimentally observed rate constants for 1-MIm solution plotted as a function of the ligand-to-zinc molar ratio under constant conditions (pH 9, CO_2-saturated, 1 atm, 25 °C) (open circles with experimental error bars). Predicted rate constants from DFT + CC speciation model (solid line); $[L]_{free}$ is represented by the dashed line accounting for mass balance with all ligands complexed to zinc. (B) Species population per ligand:Zn molar ratio.

Modeling the speciation of Zn complexes with literature-derived stepwise log *K*'s and water-bound Zn-complex pK_a values for 1-methylimidazole (1-MIm), as reported by Appleton and Sarkar,[37] indicates that, at the observed catalytically optimal ratio (15:1), ∼49% of the zinc in solution exists in three catalytically active hydroxo forms (Figure 5). Overall, the speciation equilibria include L:Zn ratios up to $[ZnL_6]^{2+}$ (L_x represents the number of complexed monodentate imidazolic ligands). In this distribution of species, $[ZnL_2(OH)(H_2O)]^+$, $[ZnL_3(OH)]^+$, and $[ZnL_4(OH)]^+$ are the predominant hydroxo forms at pH 9. We compute that, at 15:1 molar ratio ligand:Zn, 24% of the total zinc complexes are $[ZnL_2(OH)(H_2O)]^+$, with water completing the tetrahedral zinc geometry; ∼6% is in the form of $[ZnL_3(OH)]^+$; and ∼19% exists as $[ZnL_4(OH)]^+$ (see Supporting Information for mass balances and algorithms; see Appleton and Sarkar[37] for potentiometrically derived stepwise

Table 2. Measured Rate Constants (k_{obs}) Normalized for pH ($k_{int,exp}$) and Predicted ($k_{int,pred}$) for Three Monodentate Ligands Identified from the ChEMBL Database and 1-Methylimidazole (L16), Which Also Serves as a Literature Comparison (Evaluated at a 4:1 Ligand:Zn Ratio and pH 9)[a]

ligand ($[ZnL_3(OH)]^+$)	k_{obs} (M^{-1} s^{-1})	$k_{int,exp}$ (M^{-1} s^{-1})	$k_{int,pred}$ (M^{-1} s^{-1})
2-methylimidazole	108 ± 4	124 ± 5	809
Imidazole	87 ± 4	94 ± 4	676
1-methylimidazole	79 ± 19	86 ± 21	622
2,6-dichloropurine	68 ± 15	73 ± 16	406

[a]Species designation $[ZnL_3(OH)]^+$ denotes the representative stoichiometry used for ΔG_{bind} modeling prior to the speciation analysis below.

Downloaded from pubs.acs.org/acscatal/article-pdf/16/21/21140/6896732/cs-2026-038616.pdf by UNIV OF CALIFORNIA BERKELEY user on 13 November 2026

https://doi.org/10.1021/acscatal.6c03861
ACS Catal. 2026, 16, 21140−21150

stability constants (β values) used to construct Zn-imidazole speciation).

After applying the DFT + CC workflow to the various zinc species at pH 9, the speciation-weighted predicted rate constant is determined by eq 2:

$$k_{\text{pred,solution}} = \Sigma f_i \cdot k_{\text{i,pred}} \quad (2)$$

in which $k_{\text{pred,solution}}$ is the speciation-weighted predicted rate constant; f_i is the equilibrium molar fraction of each catalytically active Zn present (e.g., $[ZnL_2(OH)(H_2O)]^+$, $[ZnL_3(OH)]^+$, $[ZnL_4(OH)]^+$); and $k_{\text{i,pred}}$ is the rate constant predicted for each species *i*.

Each species $[ZnL_2(OH)(H_2O)]^+$, $[ZnL_3(OH)]^+$, and $[ZnL_4(OH)]^+$ is predicted to react with distinct rate constants of 68, 622, and 1900 M^{-1} s^{-1}, respectively (from ΔG_{bind}).

Figure 5 shows these predicted results and the experimental values for all studied compositions. The intrinsic rate constant predicted for $[ZnL_4(OH)]^+$ exceeds the highest reported value of 868 M^{-1} s^{-1} (cyclam) for the tri- and tetradentate ligand systems that dominate the literature (Figure 3). This large value indicates that simple monodentate scaffolds can achieve high intrinsic catalytic activity, although the value is not immediately apparent from the value of k_{obs}, due to unfavorable and complex speciation. The flexibility of monodentate assemblies likely permits reorganization during catalysis, enabling access to more favorable $\Sigma E^{(2)}$ (enhanced donor−acceptor stabilization), q_{Zn}, and lower $\%V_{\text{buried}}$ values than those of the ground-state geometries of rigid scaffolds.

When the speciation is fully considered and applied to the predicted results for 1-MIm (Table 2), the discrepancy at 4:1 ligand:Zn is reduced from a ∼7× overprediction to roughly a 2× underprediction of the rate constant. The ∼2× underprediction observed at 15:1 ligand:Zn can be partly attributed to systematic differences between the literature data-derived regression used to convert ΔG_{bind} to k_{int} (Figure 3) and our measured rate constants. Specifically, for cyclen and cyclam, the rate constants measured here are ∼25% and ∼10% higher, respectively, than the corresponding literature values used to construct the model (Table S1). As a result, predicted rate constants based on the literature correlation are expected to be systematically lower than those observed experimentally.

The data reported by Appleton and Sarkar[37] were obtained under conditions that differ in several respects from those used here. In their study, Zn concentrations (≈0.3 mM) are comparable to those used in this work (0.25−1 mM), but the ligand concentration is higher (77 mM 1-methylimidazole in Appleton vs ≤15 mM at the 15:1 optimum in this work). Their measurements were performed in unbuffered aqueous solution with 0.16 M KNO_3 as the electrolyte, whereas the present experiments were conducted in buffered solution (0.1 M AMPSO) with 0.2 M $NaClO_4$; i.e., similar ionic strengths but different electrolytes. In addition, Appleton and Sarkar[37] performed potentiometric equilibrium measurements rather than kinetic CO_2 hydration experiments, and did not report associated uncertainties. Despite these differences, their stepwise stability constants provide a useful thermodynamic basis for modeling, and, when combined with our computational framework reproduce the non-monotonic dependence of catalytic activity on ligand:Zn ratio, including a maximum followed by a decline as inactive species dominate at high ligand loadings.

Taken together, these factors define the expected range of uncertainty rather than a limitation of the underlying relationship between ΔG_{bind} and k_{int}. The concentration of excess ligand in solution ($[L]_{\text{free}}$) is included in Figure 5 as a secondary y-axis for visual comparison, consistent with Appleton and Sarkar's proposal that free ligand may influence the overall reaction.

3.5. Steric Limitations in Rigid Multidentate Systems

While ΔG_{bind} qualitatively predicts intrinsic activity for tri- and tetradentate ligands and captures rank-order trends in monodentate coordination environments, deviations from predicted behavior arise through two distinct mechanisms depending on ligand architecture: steric constraints in rigid multidentate systems and solution-phase speciation in monodentate systems. To assess how systematic modification of the cyclen ligand can influence intrinsic rate constants, a series of 18 Zn complexes ligated by mono-substituted cyclens containing electron withdrawing and donating functional groups was constructed. Each ligand features a single pendant group attached to a nitrogen donor atom, preserving the tetraazamacrocyclic coordination core. Rate constants were predicted using the $\Delta G_{\text{bind}} \rightarrow k_{\text{int}}$ model represented in Figure 3 for all 18 substituted compounds and expressed relative to baseline Zn-cyclen activity (set to 100%). The results plotted in Figure 6 span substitutions within a single scaffold. Across Table 1, intrinsic second-order rate constants range from zero to 868 M^{-1} s^{-1} and the values of ΔG_{bind} range from 10.0 to 22.5 kcal mol^{-1}. These rate constants and values of ΔG_{bind} are used to rank activity within this catalyst class.

Substituents leading to enhanced predicted rate constants fell into two categories: alkyl chains (e.g., butyl, propyl) and benzyl groups with electron-rich aryl rings (e.g., *para*-methoxybenzyl, *para*-hydroxybenzyl). The substituents with the largest influence are predicted to increase activity by 30−40% over the $k_{\text{int,pred}}$ of the Zn-cyclen complex. In contrast, the (4-pyridinyl)-methyl substituent is predicted to lead to a 41% decrease in rate constant. These effects were mirrored by modest changes in the Zn natural bond orbital (NBO) charge available in Table S4, which correlated with the rate constant when two outliers were excluded ($R^2 = 0.73$), suggesting that substituent effects in this subset are at least partly associated with electronic modulation of the metal center.

To test these predictions, rate constants were measured for four cyclen complexes: Zn−cyclen (unsubstituted), butyl cyclen, hexyl cyclen, and benzyl cyclen. Within this *N*-functionalized cyclen series, ΔG_{bind} predicts the experimental ranking; however, the catalyst containing unfunctionalized cyclen is more reactive than those containing all three substituted derivatives, contrary to prediction (predicted: Hexyl > Butyl > Benzyl > Cyclen; observed: Cyclen > Hexyl > Butyl > Benzyl). Ground-state $\%V_{\text{buried}}$ trends inversely with activity, as seen in Table 3. Cyclen ($\%V_{\text{buried}} = 55.4\%$) is the sterically least encumbered and experimentally most catalytically active; benzyl-cyclen ($\%V_{\text{buried}} = 62.0\%$) is experimentally least catalytically active. This outcome contrasts with the monodentate imidazole series (Table 2), in which ΔG_{bind} correlates directly with $k_{\text{int,exp}}$.

Downloaded from pubs.acs.org/acscatal/article-pdf/16/21/21140/6896732/cs-2026-038616.pdf by UNIV OF CALIFORNIA BERKELEY user on 13 November 2026

https://doi.org/10.1021/acscatal.6c03861
ACS Catal. 2026, 16, 21140−21150

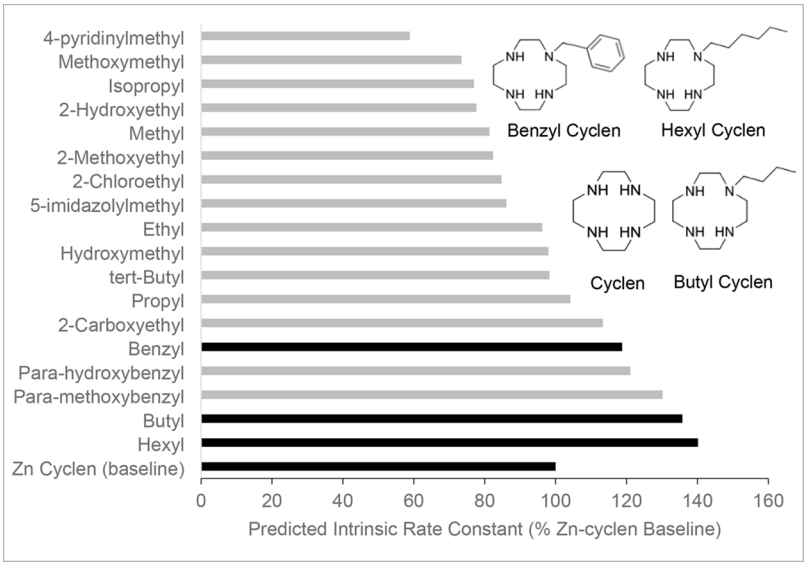


Figure 6. Predicted relative intrinsic rate constants for a series of *N*-substituted Zn-cyclen complexes based on ΔG_{bind}, without accounting for steric perturbations. Percent values represent k_{int} relative to baseline Zn-cyclen expressed as a percentage, calculated using ΔG_{bind} and the linear correlation established in Figure 3. Images of ligands experimentally tested are shown and plotted in black.

Table 3. Experimental Intrinsic Rate Constants ($k_{int,exp}$), Predictions from ΔG_{bind} ($k_{int,pred}$), and Ground-State Steric Congestion ($\%V_{buried}$) and Its Difference from That of Zn−Cyclen ($\Delta\%V_{buried}$) for *N*-Functionalized Cyclen Complexes (pH 9, 25 °C)

ligand	k_{obs} (M^{-1} s^{-1})	$k_{int,exp}$ (M^{-1} s^{-1})	$k_{int,pred}$ (M^{-1} s^{-1})	$\%V_{buried}$	$\Delta\%V_{buried}$
cyclen	662 ± 47	704 ± 50	406	55.4	0
hexyl	558 ± 47	628 ± 53	568	59.9	4.5
butyl	379 ± 34	427 ± 38	551	61.6	6.2
benzyl	364 ± 31	410 ± 35	482	62.0	6.6

We attribute the qualitative accuracy difference between the monodentate study (Table 2) and this cyclen study (Table 3) to the rigidity of the cyclen scaffold. Here, ground-state geometries do not fully capture the steric constraints experienced along the reaction coordinate and near the transition state. The ligand environment in complexes of flexible monodentate systems can more readily reorganize during catalysis. In contrast, the tetradentate cyclen framework is conformationally constrained, and pendant *N*-substituents lead to steric effects that are not as readily relieved by changes to the conformation. Under these conditions, ground-state $\Delta\%V_{buried}$ becomes more kinetically relevant than electronic parameters. This readily calculable variable $\Delta\%V_{buried}$ can be applied as a first-order perturbation to ΔG_{bind} for screening diverse scaffolds or within varied ligand families where explicit steric evaluation is warranted.

Visually represented in Figure 7, panel A, the ΔG_{bind} model applied to the four *N*-functionalized cyclen derivatives yields $R^2 = -0.76$ with an RMSE of 170 M^{-1} s^{-1}. However, panel B shows that the deviations between $k_{int,exp}$ and $k_{int,pred}$ correlate with steric congestion, captured by $\Delta\%V_{buried}$. $\Delta\%V_{buried}$ is the difference between the $\%V_{buried}$ of each complex and that of Zn−cyclen (Table 3); the $\%V_{buried}$ calculations are described in Section 2. Thus, incorporation of the steric correction term based on $\Delta\%V_{buried}$ improves agreement between $k_{int,exp}$ and $k_{int,pred}$ within this four-member series to $R^2 = 0.96$ with an RMSE of 25 M^{-1} s^{-1} and, importantly, recovers the experimental rank order (Figure 7C). Although derived from a limited data set within a single ligand class, this readily obtainable parameter can be applied to ΔG_{bind}-based screening in rigid multidentate systems, where explicit steric evaluation becomes necessary to maintain predictive accuracy.

4. CONCLUSIONS

The literature rate constants (k_{obs}) for CO_2 hydration catalyzed by Zn complexes, converted to intrinsic rate constants ($k_{int,exp}$) by accounting for the catalytically active Zn-OH fraction, are strongly associated with DLPNO-refined Zn−bicarbonate binding free energies (ΔG_{bind}) across the compiled ligand set. This relationship is retained as a bounded empirical descriptor and does not assign one universal turnover-limiting elementary step. By comparison, the first-coordination-sphere descriptors $\Sigma E^{(2)}$, q_{Zn}, and $\%V_{buried}$ give a weaker descriptive fit; their associations are reported without causal interpretation or extrapolation beyond the sampled ranges.

Although ΔG_{bind} proved generally useful as a single parameter to predict $k_{int,exp}$, the distribution of Zn-ligand complexes in solution needed to be considered to reduce a near order of magnitude discrepancy between the $k_{int,exp}$ and $k_{int,pred}$ values for reactions catalyzed by Zn complexes of monodentate ligands. Furthermore, a correction for steric hindrance of the ligand

https://doi.org/10.1021/acscatal.6c03861
ACS Catal. 2026, 16, 21140−21150

Downloaded from pubs.acs.org/acscatal/article-pdf/16/21/21140/6896732/cs-2026-038616.pdf by UNIV OF CALIFORNIA BERKELEY user on 13 November 2026

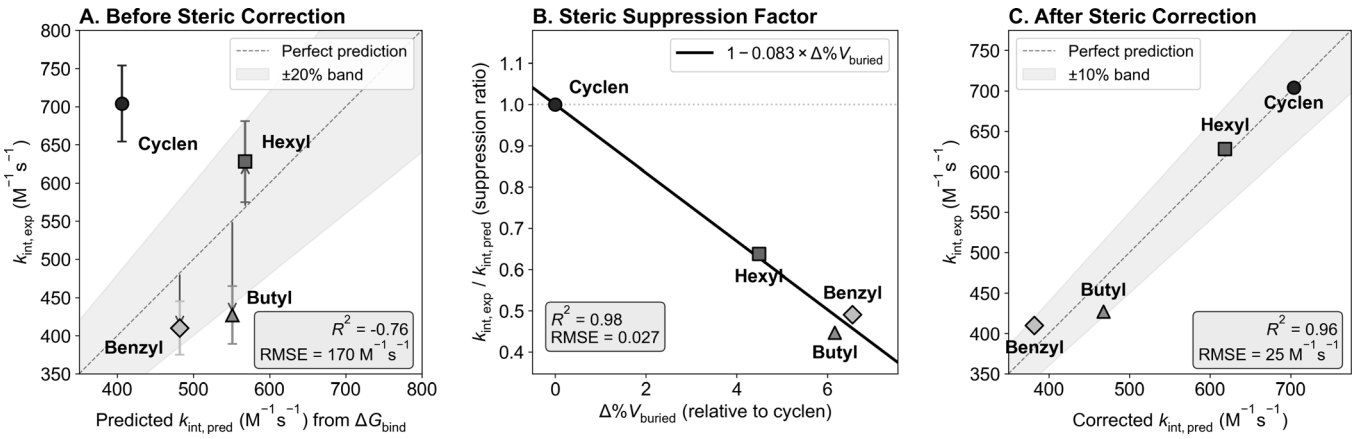


Figure 7. Evaluation of steric contribution to discrepancy between electronic descriptor predictions and experimental rate constants. Panel A shows deviation between predictions and observations ($k_{int,exp}$ vs $k_{int,pred}$) with experimental error bars. Panel B represents the formulation of the steric correction factor as a function of $\Delta\%V_{buried}$. Panel C shows corrected predicted rate constants using combined steric and electronic descriptor predictions, demonstrating substantially improved agreement between predicted and experimental values.

($\Delta\%V_{buried}$) was important to predict the trends in reactivity of cyclen ligands containing a pendant group on a coordinating nitrogen. Together, these results define a predictive framework in which ΔG_{bind}, with necessary adjustments made for steric effects and speciation of the catalytic complexes, provides a basis for the design and evaluation of Zn-based CO_2 hydration catalysts.

The most active complexes do not share a single ligand topology. Across this data set, higher activity is associated primarily with lower ΔG_{bind}. Within the regression built from the three parameters that describe the first coordination sphere (eq 1), stronger ligand-to-Zn electron donation and a less positive Zn center are associated with higher rate constants. Steric effects are scaffold-dependent: greater $\%V_{buried}$ across the multidentate set is consistent with promotion of bicarbonate displacement, whereas increasing steric encumbrance within rigid, substituted cyclens correlates with lower activity. Within the sampled chemical space, complexes reacting with higher intrinsic rate constants, therefore, combine weak product binding and strongly electron-donating ligands with steric pressure that promotes product release.

■ ASSOCIATED CONTENT

Data Availability Statement

The scripts used to evaluate the equations in this work are available at Zenodo, DOI: 10.5281/zenodo.21925290. All other data are available from the corresponding authors upon reasonable request.

Supporting Information

The Supporting Information is available free of charge at https://pubs.acs.org/doi/10.1021/acscatal.6c03861.

Experimental procedures for ligand synthesis, stopped-flow kinetic measurements, and buffer-factor determination; literature rate constants for Zn-cyclen, Zn-cyclam, and Zn-[12]aneN_3 complexes and background rate constants (Table S1); quantum mechanics computational procedure (Figure S1, Equation S1) and benchmark of ten DFT procedures (Table S2); normalization of rate constants for the fraction of catalytically active Zn-OH (Equation S2), pK_a prediction from Zn−OH bond lengths (Table S3, Figure S4), and calculated Zn charge, LUMO energy, and the relative rate constant for eighteen cyclen-derived ligands (Table S4); kinetic assays, initial-rate determination, and background correction (Equation S3, Figures S2 and S3); first-coordination-sphere descriptors $\Sigma E^{(2)}$, q_{Zn}, and $\%V_{buried}$ for Table 1 complexes (Table S5); ChEMBL compound identifiers and predicted rate constants for the 30 monodentate ligands of Figure 4 (Table S6); DFT versus DFT + CC performance metrics (Table S7); mathematical treatment of the Zn−methylimidazole speciation kinetic model (Equations S4−S30); nested leave-one-complex-out LASSO analysis (Table S8); data availability; and references (DOCX)

■ AUTHOR INFORMATION

Corresponding Authors

John F. Hartwig − *Chemical Sciences Division, Lawrence Berkeley National Laboratory, Berkeley, California 94720, United States; Department of Chemistry, University of California, Berkeley, California 94720, United States;* orcid.org/0000-0002-4157-468X; Email: jhartwig@berkeley.edu

Douglas S. Clark − *Department of Chemical and Biomolecular Engineering, University of California, Berkeley, California 94720, United States; Molecular Biophysics and Integrated Bioimaging Division, Lawrence Berkeley National Laboratory, Berkeley, California 94720, United States;* orcid.org/0000-0003-1516-035X; Email: dsc@berkeley.edu

Authors

Thomas Quaid − *Department of Chemical and Biomolecular Engineering, University of California, Berkeley, California 94720, United States;* orcid.org/0009-0007-4691-9310

Cooper Citek − *Chemical Sciences Division, Lawrence Berkeley National Laboratory, Berkeley, California 94720, United States*

Complete contact information is available at: https://pubs.acs.org/doi/10.1021/acscatal.6c03861

https://doi.org/10.1021/acscatal.6c03861
ACS Catal. 2026, 16, 21140−21150

Downloaded from pubs.acs.org/acscatal/article-pdf/16/21/21140/6896732/cs-2026-038616.pdf by UNIV OF CALIFORNIA BERKELEY user on 13 November 2026

Author Contributions

D.S.C. supervised this work. T.Q. prepared the manuscript. D.S.C., T.Q., C.C., and J.F.H. edited the manuscript. T.Q. developed the methodology, performed the modeling, and analyzed the kinetic data. C.C. prepared the Zn compounds and carried out the kinetic measurements.

Notes

The authors declare no competing financial interest.

■ ACKNOWLEDGMENTS

This work was supported by Fifth Generation, Inc. and by the U.S. Department of Energy, Office of Science, Basic Energy Sciences, Chemical Sciences, Geosciences, and Biosciences Division under Contract No. DE-AC02-05-CH11231 within the Lawrence Berkeley National Laboratory (LBNL) Catalysis Program (CH030201). Experimental work, including stopped-flow kinetics measurements and material preparation carried out in the LBNL Catalysis Laboratory, as well as data interpretation and manuscript preparation, was conducted under Contract DE-AC02-05-CH11231, FWP CH030201. Computational work, including method development, calculations, and data analysis, was funded by Fifth Generation, Inc.

■ REFERENCES

(1) Petrik, I. D.; Liu, J.; Lu, Y. Metalloenzyme Design and Engineering through Strategic Modifications of Native Protein Scaffolds. *Curr. Opin. Chem. Biol.* **2014**, *19*, 67−75.

(2) Valdez, C. E.; Smith, Q. A.; Nechay, M. R.; Alexandrova, A. N. Mysteries of Metals in Metalloenzymes. *Acc. Chem. Res.* **2014**, *47* (10), 3110−3117.

(3) Himiyama, T.; Okamoto, Y. Artificial Metalloenzymes: From Selective Chemical Transformations to Biochemical Applications. *Molecules* **2020**, *25* (13), 2989.

(4) Angeli, A.; Carta, F.; Supuran, C. T. Carbonic Anhydrases: Versatile and Useful Biocatalysts in Chemistry and Biochemistry. *Catalysts* **2020**, *10* (9), 1008.

(5) Zhou, Y.; Wang, Y.; Chen, Z.; Gong, H.; Chen, L.; Yu, H. Highly Hydrophilic ZIF-8 as a Carbonic Anhydrase Mimetic Catalyst for Promoting CO_2 Absorption. *J. Phys. Chem. C* **2023**, *127* (15), 7184−7196.

(6) Lindskog, S. Structure and Mechanism of Carbonic Anhydrase. *Pharmacol. Ther.* **1997**, *74* (1), 1−20.

(7) Domsic, J. F.; Avvaru, B. S.; Kim, C. U.; Gruner, S. M.; Agbandje-McKenna, M.; Silverman, D. N.; McKenna, R. Entrapment of Carbon Dioxide in the Active Site of Carbonic Anhydrase II. *J. Biol. Chem.* **2008**, *283* (45), 30766−30771.

(8) Alvizo, O.; Nguyen, L. J.; Savile, C. K.; Bresson, J. A.; Lakhapatri, S. L.; Solis, E. O. P.; Fox, R. J.; Broering, J. M.; Benoit, M. R.; Zimmerman, S. A.; Novick, S. J.; Liang, J.; Lalonde, J. J. Directed Evolution of an Ultrastable Carbonic Anhydrase for Highly Efficient Carbon Capture from Flue Gas. *Proc. Natl. Acad. Sci. U. S. A.* **2014**, *111* (46), 16436−16441.

(9) Rigkos, K.; Filis, G.; Antonopoulou, I.; de Oliveira Maciel, A.; Saridis, P.; Zarafeta, D.; Skretas, G. Biomimetic CO_2 Capture Unlocked through Enzyme Mining: Discovery of a Highly Thermo- and Alkali-Stable Carbonic Anhydrase. *Environ. Sci. Technol.* **2024**, *58* (40), 17732−17742.

(10) Verma, M.; Bhaduri, G. A.; Phani Kumar, V. S.; Deshpande, P. A. Biomimetic Catalysis of CO_2 Hydration: A Materials Perspective. *Ind. Eng. Chem. Res.* **2021**, *60* (13), 4777−4793.

(11) Floyd, W. C., III; Baker, S. E.; Valdez, C. A.; Stolaroff, J. K.; Bearinger, J. P.; Satcher, J. H., Jr.; Aines, R. D. Evaluation of a Carbonic Anhydrase Mimic for Industrial Carbon Capture. *Environ. Sci. Technol.* **2013**, *47* (17), 10049−10055.

(12) Brown, R. S.; Salmon, D.; Curtis, N. J.; Kusuma, S. Carbonic Anhydrase Models. 4. [Tris[(4,5-Dimethyl-2-Imidazolyl)Methyl]Phosphine Oxide]Cobalt(2+), a Small-Molecule Mimic of the Spectroscopic Properties of Cobalt(II) Carbonic Anhydrase. *J. Am. Chem. Soc.* **1982**, *104* (11), 3188−3194.

(13) Kimura, E.; Shiota, T.; Koike, T.; Shiro, M.; Kodama, M. A Zinc(II) Complex of 1,5,9-Triazacyclododecane ([12]aneN3) as a Model for Carbonic Anhydrase. *J. Am. Chem. Soc.* **1990**, *112* (15), 5805−5811.

(14) Park, D.; Lee, M. S. Kinetic Study of CO_2 Hydration by Small-Molecule Catalysts with a Second Coordination Sphere That Mimic the Effect of the Thr-199 Residue of Carbonic Anhydrase. *Biomimetics* **2019**, *4* (4), 66.

(15) Rains, J. G. D.; O'Donnelly, K.; Oliver, T.; Woscholski, R.; Long, N. J.; Barter, L. M. C. Bicarbonate Inhibition of Carbonic Anhydrase Mimics Hinders Catalytic Efficiency: Elucidating the Mechanism and Gaining Insight toward Improving Speed and Efficiency. *ACS Catal.* **2019**, *9* (2), 1353−1365.

(16) Kim, J. Y.; Kulik, H. J. When Is Ligand pK_a a Good Descriptor for Catalyst Energetics? In Search of Optimal CO_2 Hydration Catalysts. *J. Phys. Chem. A* **2018**, *122* (18), 4579−4590.

(17) Koziol, L.; Valdez, C. A.; Baker, S. E.; Lau, E. Y.; Floyd, W. C., III; Wong, S. E.; Satcher, J. H., Jr.; Lightstone, F. C.; Aines, R. D. Toward a Small Molecule, Biomimetic Carbonic Anhydrase Model: Theoretical and Experimental Investigations of a Panel of Zinc(II) Aza-Macrocyclic Catalysts. *Inorg. Chem.* **2012**, *51* (12), 6803−6812.

(18) Liu, M.; Nazemi, A.; Taylor, M. G.; Nandy, A.; Duan, C.; Steeves, A. H.; Kulik, H. J. Large-Scale Screening Reveals That Geometric Structure Matters More Than Electronic Structure in the Bioinspired Catalyst Design of Formate Dehydrogenase Mimics. *ACS Catal.* **2022**, *12* (1), 383−396.

(19) Lan, G.; Fan, Y.; Shi, W.; You, E.; Veroneau, S. S.; Lin, W. Biomimetic Active Sites on Monolayered Metal−Organic Frameworks for Artificial Photosynthesis. *Nat. Catal.* **2022**, *5* (11), 1006−1018.

(20) Ma, R.; Schuette, G. F.; Broadbelt, L. J. Microkinetic Modeling of CO_2 Hydrolysis over Zn-(1,4,7,10-Tetraazacyclododecane) Catalyst Based on First Principles: Revelation of Rate-Determining Step. *J. Catal.* **2014**, *317*, 176−184.

(21) Reed, A. E.; Weinstock, R. B.; Weinhold, F. Natural Population Analysis. *J. Chem. Phys.* **1985**, *83* (2), 735−746.

(22) Glendening, E. D.; Landis, C. R.; Weinhold, F. Natural Bond Orbital Methods. *WIREs Comput. Mol. Sci.* **2012**, *2* (1), 1−42.

(23) Clavier, H.; Nolan, S. P. Percent Buried Volume for Phosphine and N-Heterocyclic Carbene Ligands: Steric Properties in Organometallic Chemistry. *Chem. Commun.* **2010**, *46* (6), 841−861.

(24) Poater, A.; Cosenza, B.; Correa, A.; Giudice, S.; Ragone, F.; Scarano, V.; Cavallo, L. SambVca: A Web Application for the Calculation of the Buried Volume of N-Heterocyclic Carbene Ligands. *Eur. J. Inorg. Chem.* **2009**, *2009* (13), 1759−1766.

(25) Neese, F. The ORCA Program System. *WIREs Comput. Mol. Sci.* **2012**, *2*, 73−78.

(26) Neese, F. Software Update: The ORCA Program System, Version 6.0. *WIREs Comput. Mol. Sci.* **2025**, *15* (2), e70019.

(27) Sobez, J.-G.; Reiher, M. Molassembler: Molecular Graph Construction, Modification, and Conformer Generation for Inorganic and Organic Molecules. *J. Chem. Inf. Model.* **2020**, *60* (8), 3884−3900.

(28) Bannwarth, C.; Ehlert, S.; Grimme, S. GFN2-xTB—An Accurate and Broadly Parametrized Self-Consistent Tight-Binding Quantum Chemical Method with Multipole Electrostatics and Density-Dependent Dispersion Contributions. *J. Chem. Theory Comput.* **2019**, *15* (3), 1652−1671.

(29) Pracht, P.; Grimme, S.; Bannwarth, C.; Bohle, F.; Ehlert, S.; Feldmann, G.; Gorges, J.; Müller, M.; Neudecker, T.; Plett, C.; Spicher, S.; Steinbach, P.; Wesołowski, P. A.; Zeller, F. CREST—A Program for the Exploration of Low-Energy Molecular Chemical Space. *J. Chem. Phys.* **2024**, *160* (11), 114110.

Downloaded from pubs.acs.org/acscatsc/article-pdf/16/21/21140/6896732/cs-2026-038616.pdf by UNIV OF CALIFORNIA BERKELEY user on 13 November 2026

https://doi.org/10.1021/acscatal.6c03861
ACS Catal. 2026, 16, 21140−21150

(30) Satcher, J. H.; Baker, S. E.; Kulik, H. J.; Valdez, C. A.; Krueger, R. L.; Lightstone, F. C.; Aines, R. D. Modeling, Synthesis and Characterization of Zinc Containing Carbonic Anhydrase Active Site Mimics. *Energy Procedia* **2011**, *4*, 2090−2095.
(31) Zhang, X.; van Eldik, R. A Functional Model for Carbonic Anhydrase: Thermodynamic and Kinetic Study of a Tetraazacyclododecane Complex of Zinc(II). *Inorg. Chem.* **1995**, *34* (22), 5606−5614.
(32) Ma, R.; Schuette, G. F.; Broadbelt, L. J. Catalyst Screening through Quantum Chemical Calculations and Microkinetic Modeling: Hydrolysis of Carbon Dioxide. *Theor. Found. Chem. Eng.* **2017**, *51* (6), 949−960.
(33) de Souza, B. GOAT: A Global Optimization Algorithm for Molecules and Atomic Clusters. *Angew. Chem., Int. Ed.* **2025**, *64* (18), e202500393.
(34) Yadav, N.; Singh Chundawat, T. Recent Trends on Zinc Complexes Bearing Bi-, Tri- and Tetra-Dentate Schiff Base Ligands for Catalytic Ring-Opening Polymerization of Lactides. *ChemistrySelect* **2024**, *9* (34), e202401619.
(35) Huang, D.; Makhlynets, O. V.; Tan, L. L.; Lee, S. C.; Rybak-Akimova, E. V.; Holm, R. H. Fast Carbon Dioxide Fixation by 2,6-Pyridinedicarboxamidato-Nickel(II)-Hydroxide Complexes: Influence of Changes in Reactive Site Environment on Reaction Rates. *Inorg. Chem.* **2011**, *50* (20), 10070−10081.
(36) Liao, W.; Liu, P. Enhanced Descriptor Identification and Mechanism Understanding for Catalytic Activity Using a Data-Driven Framework: Revealing the Importance of Interactions between Elementary Steps. *Catal. Sci. Technol.* **2022**, *12* (12), 3836−3845.
(37) Appleton, D. W.; Sarkar, B. The Activity-Related Ionization in Carbonic Anhydrase. *Proc. Natl. Acad. Sci. U. S. A.* **1974**, *71* (5), 1686−1690.

Downloaded from pubs.acs.org/accacs/article-pdf/16/21/21140/6896732/cs-2026-038616.pdf by UNIV OF CALIFORNIA BERKELEY user on 13 November 2026

https://doi.org/10.1021/acscatal.6c03861
ACS Catal. 2026, 16, 21140−21150